Surface film formation on a graphite electrode in Li-ion batteries: AFM and XPS study

ARTICLE *in* SURFACE AND INTERFACE ANALYSIS · OCTOBER 2005

Impact Factor: 1.25 · DOI: 10.1002/sia.2072

SURFACE AND INTERFACE ANALYSIS
Surf. Interface Anal. 2005; **37**: 773–781
Published online 28 July 2005 in Wiley InterScience (www.interscience.wiley.com). DOI: 10.1002/sia.2072

SIA

Surface film formation on a graphite electrode in Li-ion batteries: AFM and XPS study

S. Leroy,[1] F. Blanchard,[2] R. Dedryvère,[1]* H. Martinez,[1] B. Carré,[2] D. Lemordant[2] and D. Gonbeau[1]

[1] LCTPCM, Université de Pau, Hélioparc Pau Pyrénées, 64053 Pau Cedex 9, France
[2] P.I.M.I.R. (EA 2098), Faculté des Sciences de Tours, Parc de Grandmont, 37000 Tours, France

Received 21 February 2005; Revised 16 June 2005; Accepted 16 June 2005

The formation of a passivation film (solid electrolyte interphase, SEI) at the surface of the negative electrode of full $LiCoO_2$/graphite lithium-ion cells using $LiPF_6$ (1M) in carbonate solvents as electrolyte was investigated by means of x-ray photoelectron spectroscopy (XPS) and atomic force microscopy (AFM). The analyses were carried out at different potentials of the first and the fifth cycles, showing the potential-dependent character of the surface-film species formation. These species were mainly identified as Li_2CO_3 up to 3.8 V and LiF up to 4.2 V. This study shows the formation of the SEI during charging and its partial dissolution during discharge. Copyright © 2005 John Wiley & Sons, Ltd.

KEYWORDS: Li-ion battery; graphite; electrode/electrolyte interface; XPS; AFM

INTRODUCTION

Graphite is the material of choice for negative electrodes of lithium-ion batteries, which are the most efficient power sources of today's portable electronics. Numerous research works have shown that the performances of Li-ion batteries using graphite as negative electrode are closely linked to complex phenomena occurring at the electrode–electrolyte interface. Indeed, the layered structure of graphite can be easily affected by side reactions such as cointercalation of species from the electrolyte together with Li^+ ions, leading to the exfoliation of graphene planes and the deactivation of the electrode.[1] Therefore, the stability of the graphite electrode strongly depends on the formation of a protective passivation film on its surface, called *solid electrolyte interphase* (SEI).[2,3] It is generally admitted that the retention capacity and storage life of the Li-ion batteries directly depend on the stability of the SEI, and that Li^+ ions can reversibly intercalate/de-intercalate into graphite only when a stable SEI is formed. Moreover, it dramatically reduces the kinetics of the electrolyte decomposition and further active lithium consumption by making a physical barrier between the lithiated carbon electrode and the binder reactants. Therefore, the formation of the SEI has been recognized to be an essential process in the manufacture of Li-ion batteries. It was shown that the formation of the SEI originates from the reductive decomposition of the solvents and salt during the initial few charge/discharge cycles of the battery.[4–6] However, its mechanism of formation as well as its composition and nature are still subject to numerous controversial discussions, and still monopolize a lot of research efforts. Common electrolytes consist of $LiPF_6$ dissolved in a mixture of alkyl carbonate solvents, and so the decomposition products making up the SEI are usually identified as LiF, Li_2CO_3 or lithium alkyl carbonates $ROCO_2Li$.[7,8]

The most common characterization techniques used to identify the organic/inorganic compounds formed at the electrode–electrolyte interfaces are Fourier-transform infrared spectroscopy (FTIR)[9,10] and X-ray photoelectron spectroscopy (XPS),[11,12] and many studies have dealt with the influence of the solvent and salt nature on the SEI formation using both techniques. However, to our knowledge, no study reports a systematic work in XPS combining core peaks and valence-band analysis at different stages of the discharge or charge. The theme of this paper is to further investigate the processes of formation of the SEI step by step during the electrochemical insertion of lithium ions into graphite using two experimental techniques: atomic force microscopy (AFM) and XPS, which together provide a suitable surface analysis approach. XPS coupled with AFM enabled us to propose a composition of the SEI together with its nanoscale morphological description. More precisely, to distinguish the processes induced by simple contact of the electrode with the electrolyte from processes occurring only during cycling, our study is organized as follows:

(1) First, the formation of a film at the surface of the electrode by simple contact with the electrolyte will be considered, by comparison with highly oriented pyrolytic graphite (HOPG).
(2) Then the formation of the SEI during cycling will be investigated at different potentials of the first and the fifth charges.

*Correspondence to: R. Dedryvère, LCTPCM, Université de Pau, Hélioparc Pau Pyrénées, 2 av. Pierre Angot, 64053 Pau Cedex 9, France. E-mail: remi.dedryvere@univ-pau.fr
Contract/grant sponsor: French Regional Center.

EXPERIMENTAL

Sample preparation

The graphite electrodes, a mixture of synthetic graphite flakes ($d_{50} = 22\,\mu m$) and mesocarbon microbeads (MCMB, $d_{50} = 10.2\,\mu m$), were kindly provided by SAFT, who also provided the cobalt electrodes ($LiCoO_2$). The active material of the negative electrode was deposited on a Cu foil. For mechanical stability, the graphite powder was mixed with two binders: styrene butadiene rubber (SBR) and carboxymethyl cellulose (CMC). The electrolyte EC/DEC/DMC (2/2/1) (ethylene, diethyl and dimethyl carbonates) + $LiPF_6$ (1M) was purchased from Merck (Selectipur®) and the water content of the solvents was less than 20 ppm as indicated by the manufacturer. Graphite/Li_xCoO_2 cells were built using Swagelok connectors and cycled with an Arbin battery cycler. Charge and discharge cycles were operated in the galvanostatic mode at C/20 rate with a current density of 177 $\mu A\ cm^{-2}$ (a C/20 rate corresponds to a current density at which the full capacity of the cell can be charged – or discharged – in 20 h). Charge was operated to a cut-off voltage of +4.3 V and discharge to a cut-off voltage of +2.5 V.

For surface studies during cycling, the negative electrodes were carefully separated from the rest of the battery components, washed with DMC to remove the electrolyte, and dried prior to being packed into a hermetically sealed glass tube for transportation. All the operation was done in a glove box under argon atmosphere.

XPS measurements

To prevent the samples from moisture/air exposure on the analysis site, the XPS spectrometer was directly connected through a transfer chamber to a nitrogen dry-box so that the electrodes could be easily removed from the tube within the dry-box, and placed on the sample holder without any contamination.

XPS analyses were carried out with a Kratos Axis Ultra spectrometer using a focused monochromatized Al Kα radiation ($h\nu = 1486.6$ eV). The spectrometer was calibrated using the photoemission line Ag $3d_{5/2}$ (binding energy 368.3 eV). For the Ag $3d_{5/2}$ line, the full width at half maximum (FWHM) was 0.58 eV under the recording conditions. Core peaks and valence-band spectra were recorded with 20 eV constant pass energy. The analyzed area of the samples was $300 \times 700\,\mu m^2$, and the pressure in the analysis chamber was ca. 5×10^{-7} Pa. No charge neutralization was used. Short-time spectra were recorded at the beginning and at the end of each experiment to check the nondegradation of the samples in the X-ray beam. Peaks assignments were made with respect to reference compounds, namely, $LiPF_6$, LiF, Li_2CO_3, polyethylene oxide PEO $(-CH_2-CH_2-O-)_n$, CH_3OCO_2Li and $OP(OCH_3)_3$. The binding energy scale was calibrated from the carbon contamination using the C 1s peak at 285.0 eV. Core peaks were analyzed using a nonlinear Shirley-type background,[13] and peak positions and areas were obtained by a weighed least-square fitting of model curves (70% Gaussian, 30% Lorentzian) to the experimental data. Quantification was performed on the basis of Scofield's relative sensitivity factors.[14]

AFM

We imaged the samples in UHV conditions using a commercial (VP from Park Scientific Instrument) contact AFM head, controlled by feedback electronics and software of conventional design. The residual pressure inside the analysis chamber was in the 5×10^{-9} Pa range.

Typical radii of curvature of the tip were 20 nm and spring constant, 0.07 N/m. Images were recorded in the constant force mode, in the range 10–20 nN with a low scan frequency (0.5 Hz). A one-micron grill and mica, used as calibration samples, always gave the correct periodicity.

RESULTS AND DISCUSSION

First, studies were conducted on the composite electrode described above, as well as HOPG used as a reference compound.

The C 1s XPS core peak of HOPG (Fig. 1a) exhibits a typically thin and asymmetrical shape, as is regularly observed. The main differences with the anode (Fig. 1b) used in this work consist of other components located at higher binding energies: 286 and 287.8 eV, assigned respectively to C–O and C=O environments from the CMC binder.

Figure 2 shows AFM images of $10 \times 10\,\mu m^2$ areas of HOPG basal plane (Fig. 2a) and of the composite electrode (Fig. 2b). The surface of HOPG exhibits atomically flat terraces separated by several steps, which are typical AFM images of such basal planes. The surface of the composite electrode is more perturbed, with still large flat terraces but also great completely crumpled zones attributable to the binders' mass. Note that at this imaging scale, MCMB cannot be identified. Images displayed on the top left corner are STM analyses conducted on the flat terraces. Using STM, the hexagonal arrangement of graphite basal plane atoms, with a *ca.* 0.24-nm parameter, is observed. This result indisputably allows us to attribute the succession of basal planes to graphite (Fig. 2b). As only graphite basal planes are clearly identifiable, in the continuation of this work, the

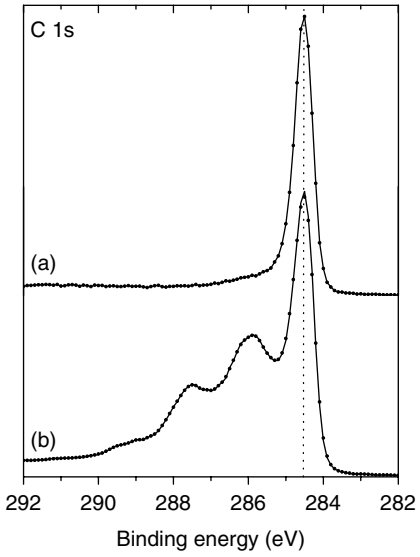

Figure 1. C 1s XPS spectra of: (a) graphite HOPG and (b) the composite electrode.

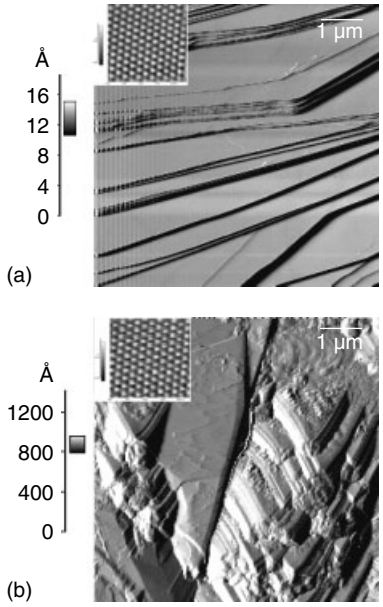

Figure 2. 10 × 10 µm^2 AFM images of: (a) HOPG and (b) the composite electrode.

SEI morphology of the composite negative electrode (from the true lithium-ion battery) investigated by scanning probe microscopy and depending of the Li intercalation rate, will be achieved on the basal plane alone.

However, in the further discussion, the XPS investigation of the SEI will not be conducted on basal planes only, because in the analyzed area (300 × 700 µm^2), graphite planes and cross sections and microbeads are simultaneously present. These last comments should be underlined because it is well established that the SEI formation mechanisms are different depending on whether it is formed on graphite basal planes or cross sections.[15] Indeed, carbon atoms of the cross sections were found to be much more active than those of the basal planes.[16]

Reactivity of the electrode

First, we analyzed the reactivity of the electrode with organic solvents contained in the electrolyte. This makes it possible to distinguish the reactivity of the electrode related to the electrolyte from that specific to the lithium salt. By comparison, the same study was undertaken on HOPG graphite, even though we were fully aware that this compound exhibits a very weak reactivity.

The electrode and graphite were put in contact with the organic solvent DMC for 24 h. No significant modification was observed for the morphology and for the chemical composition of the surfaces studied.

Under normal conditions of battery operation, the electrodes remain in contact with the electrolyte 16 h before starting cycling experiments. Soakings were therefore carried out under the same conditions. In order to better investigate the effects of dipping the electrodes in the electrolyte, the samples were either rinsed or not rinsed after soaking, before analysis.

Table 1 shows the evolution of the surface chemical composition (determined by XPS quantitative analyses) for rinsed and nonrinsed samples. These results show a strong decrease of the carbon content for the unwashed sample. At the same time, we can note the appearance of fluorine, phosphorus and lithium, corresponding to a $LiPF_6$ deposit. The rinsed electrode presents identical evolutions, with, however, a smaller amount of salt on the surface. Under the same conditions, similar results were obtained with HOPG graphite.

Table 1. Chemical composition (%) of the composite electrode's surface before and after soaking in electrolyte

Peak	Native electrode	Soaked 24 h without rinsing	Soaked 24 h and rinsed
C 1s	86	54	75
O 1s	14	6	8
F 1s	–	18	6
P 2p	–	6	2
Li 1s	–	16	9

Figure 3 presents the C 1s XPS core peaks of unwashed (3b) and washed (3c) electrodes in comparison with the native electrode (Fig. 3a). For both samples, b and c, the components located at high binding energies (286.0 and 287.8 eV) due to the binder are not detected. The F 1s (687.5 eV) and P 2p (137.9 eV) XPS core peaks (not shown here) reveal the deposit of a layer mainly made up of $LiPF_6$, with a very small amount of phosphates coming from the decomposition of the salt.

Figure 4 shows the AFM images of unwashed (4a) and washed (4b) electrodes. The surface of the unwashed electrode is completely covered by a layer as compared to the native electrode. On the other hand, the washed electrode is very similar to the native electrode.

On the whole, dipping the electrode in the electrolyte leads to the formation of a layer on the surface of the electrode. This layer mainly comes from $LiPF_6$ contained

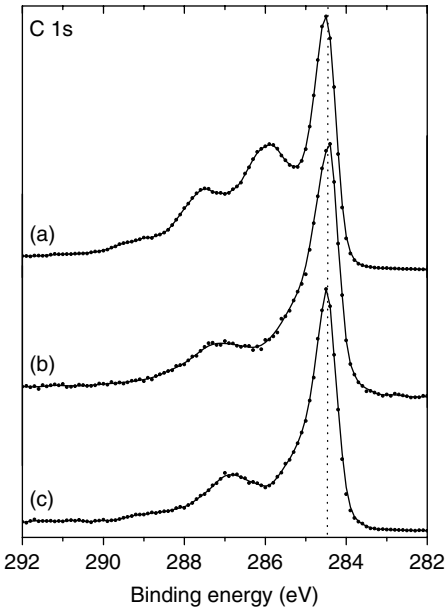

Figure 3. C 1s XPS spectra of: (a) the native composite electrode, and of the electrode soaked for 24 h in the electrolyte (b) without rinsing and (c) rinsed by DMC.

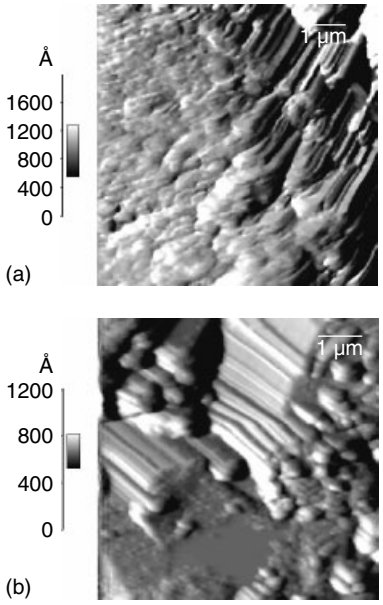

Figure 4. 10 × 10 µm^2 AFM images of the electrode soaked for 24 h in the electrolyte (a) without rinsing and (b) rinsed by DMC.

in the electrolyte. Its thickness increases with the time of soaking, and the layer partially dissolves during washing.

This preliminary study was necessary to be able to identify and separate the mechanism of interface formation purely due to cycling from that due to the reactivity of the uncharged electrode with the electrolyte.

Surface study during cycling

Figure 5 shows the results of 1st and the 5th cycles of charge/discharge of electrochemical cells under the conditions described above. In each figure are represented the voltages of: (a) the operating cell ($LiCoO_2/Li_xC_6$) studied in this work, and (b) a cell made up of a Li_xC_6 cathode and a lithium anode (Li_xC_6/Li) when cycling under the same conditions, as a comparison. This comparison allows us to know the voltage of the graphite electrode *versus* Li^+/Li in the real battery during cycling. In order to analyze precisely the mechanism of the SEI layer formation at the electrode's surface, two series of samples have been prepared. For the first series, the electrochemical reaction was stopped after the first charge of the cell at 3.0 V, 3.5 V, 3.8 V and 4.2 V corresponding, for the negative graphite electrode, to 0.9 V, 0.4 V, 0.15 V and 0.01 V *versus*. Li^+/Li respectively. For the second series, the cells were cycled four times and stopped during the fifth charging at the same potentials. As noted before, each composite electrode was recovered from the cell after electrochemical reaction and washed by DMC.

The results obtained with both series of samples are now analyzed separately.

First charge

Figure 6 shows the AFM images of the composite electrode after the first charge at (a) 3.0 V and (b) 4.2 V. At the beginning of charging (Fig. 6a), the electrode exhibits platelets with sharp angles (graphite sheets) and amorphous-like regions due to the binder. It exhibits a very similar profile to the freshly prepared electrode. This can be explained by

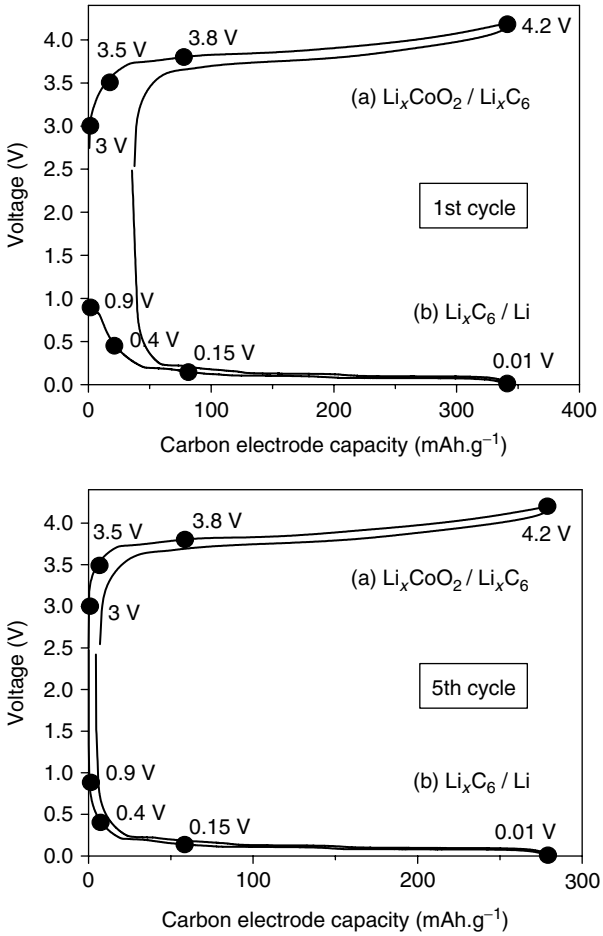

Figure 5. 1st and 5th cycles of charge/discharge of: (a) the operating cell ($LiCoO_2/Li_xC_6$) studied in this work, and (b) a cell made up of a Li_xC_6 cathode and a lithium anode (Li_xC_6/Li) as a comparison.

the fact that, at this early stage of charge, the potential of the graphite electrode is still rather high (about 0.9 V *vs*. Li^+/Li), and so the formation of the SEI has barely started. On the other hand, the electrode recovered after a full charge of the cell at 4.2 V (Fig. 6b) displays a very different surface. The sharp angles attributed to the graphite sheets are hardly detectable and most of the surface looks amorphous. This clearly shows the formation of a surface layer at the end of the charge, when the potential of the graphite electrode is very low (about 0.01 V *vs*. Li^+/Li).

Figure 7 shows the C 1s, F 1s, P 2p and Li 1s core peak spectra of composite graphite electrodes recovered from the cells after a first charge at: (a) 3.0 V, (b) 3.5 V, (c) 3.8 V and (d) 4.2 V. Results of the quantitative analysis of these samples are reported in Table 2. All spectra are reported without any fitting of the peaks, for more clarity. O 1s core peak spectra are not shown here as they provide very little information, since all oxygen-containing species present at the surface layer contribute to the observed spectrum, with very little variations in binding energy.

C 1s spectra. The spectrum of sample (a) displays a very similar profile to that of an electrode simply soaked for 24 h in the electrolyte. The narrow main peak observed at

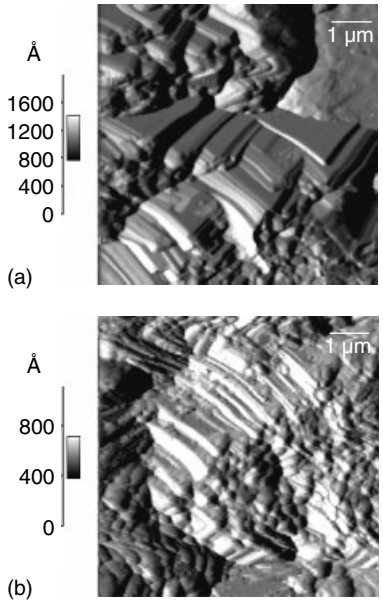

Figure 6. 10 × 10 μm^2 AFM images of the composite negative electrode stopped at (a) 3.0 V and (b) 4.2 V during the first charge.

284.5 eV is assigned to graphite, while other components mainly come from the first layer formed at the surface by soaking the electrode in the electrolyte. However, as the graphite peak is smaller, this suggests that the SEI formation process has just started. Then, upon charging and insertion of lithium ions, we can observe a progressive decrease of this peak which is hardly detectable after charge at 3.8 V and completely disappearing at 4.2 V. Taking into account the XPS depth analysis (≈5 nm), we estimate that the SEI formed at the end of the first charge is thicker than 5 nm. This result confirms the AFM observation.

In addition to the graphite peak, three main peaks can be observed during charging: the first at 285.0 eV is attributed to hydrocarbon contamination and to carbon atoms bound only to C or H atoms. The second, at 286.8 eV, is attributed to carbon atoms in a one-oxygen environment, while the third, at 290.1 eV, is assigned to carbon atoms in a three-oxygen environment. This latter one is due to the presence of carbonate species, which can be Li_2CO_3 and/or lithium alkyl carbonates $ROCO_2Li$. The peak at 286.8 eV can be attributed to carbon atoms bound to one oxygen in lithium alkyl carbonates ($R-\underline{C}H_2-OCO_2Li$). Such lithium alkyl carbonate species have been widely described as the main components of the SEI forming on graphite negative electrodes.[6,7,17] However, in $ROCO_2Li$ species the number of carbon atoms bound to three oxygens and bound to one oxygen is the same. Now, if we consider sample (b) obtained after charging at 3.5 V, the peak intensity at 286.8 eV is much higher than that at 290.1 eV. It can thus not be due only to the presence of Li alkyl carbonates species, for which both peaks would exhibit the same intensity. The peak at 286.8 eV could be explained by the presence of oligomeric species of polyethylene oxide PEO $(-CH_2-CH_2-O-)_n$, for which all carbon atoms are in a one-oxygen environment, or ROLi species. Those compounds have already been detected at the surface of various electrodes.[18–20]

After charging the cell at 3.8 V (sample c), the peak at 290.1 eV appears as more intense than that at 286.8 eV, in contrast to the previous sample. This peak is therefore mainly due to Li_2CO_3, while the small peak at 286.8 eV is explained by the presence of a small amount of Li alkyl carbonates and/or PEO oligomers.

Finally, after full charge at 4.2 V, carbon-containing species at the surface are mainly Li alkyl carbonates $ROCO_2Li$ or a mixture of $Li_2CO_3$and $ROCO_2Li$, probably associated with a small amount of PEO oligomers $(-CH_2-CH_2-O-)_n$ or ROLi species.

Note that an additional weak component (1–3%) at 288.7–289.0 eV was necessary to fully interpret the shape of these C 1s spectra (Table 2). This component can be assigned to carbon atoms in a two-oxygen environment, and can be explained by a small amount of oxalates at the surface.

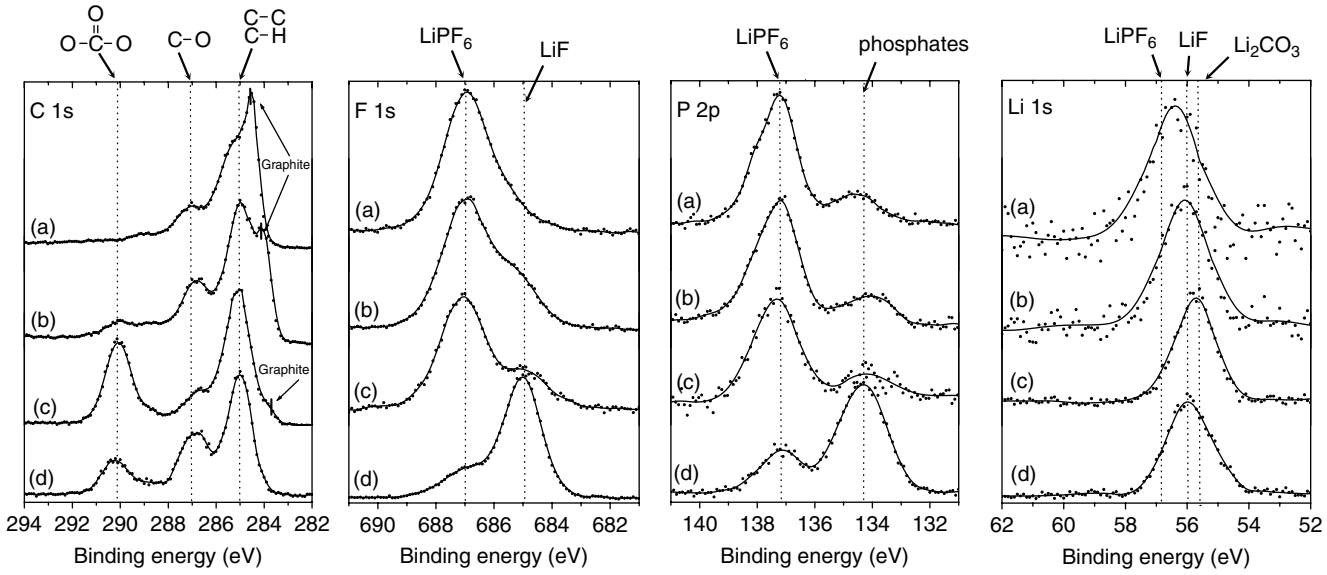

Figure 7. C 1s, F 1s, P 2p and Li 1s XPS spectra of the composite negative electrode stopped at (a) 3.0 V, (b) 3.5 V, (c) 3.8 V and (d) 4.2 V during the first charge.

Table 2. Binding energy (eV) and atomic percentage (%) of the elements C, O, F, P and Li from XPS spectra of the composite negative electrode as a function of the voltage of the cell during the 1st cycle (corresponding to Fig. 7)

	3.0 V		3.5 V		3.8 V		4.2 V	
Peak	BE (eV)	%	BE (eV)	%	BE (eV)	%	BE (eV)	%
C 1s	284.5	23	284.2	8	283.7	0.9	–	–
	285.1	27	285.0	26	285.0	16	285.0	11
	287.0	16	286.9	11	286.7	5	286.9	7
	289.0	2.9	288.8	2.7	288.7	1	288.8	1
	–	–	290.1	3.5	290.0	11	290.2	3.4
O 1s	532.2	7	532.4	12	532.6	28	531.6	20
	533.6	8	533.8	10	533.5	9	533.5	7
F 1s	684.9	1	685.1	3	684.9	1	685.0	17
	686.9	7	686.9	9	687.1	3	686.9	4
P 2p	134.5	0.4	134.1	0.6	134.2	0.2	134.3	2.6
	137.2	1.7	137.2	2.2	137.3	0.9	137.1	1
Li 1s	56.4	6	56.1	12	55.8	24	56.0	26

Their formation mechanism has been discussed in a previous work,[20] and can be due to solvent decomposition reactions leading to the formation of CO_2.

F 1s spectra. The F 1s core peaks of the same samples consist of two peaks (Fig. 7). The first one at 687.0 eV is clearly attributed to the salt $LiPF_6$, while the second one at 685.0 eV is assigned to LiF. Upon charge, we can observe an increase in LiF peak. Results of quantitative analysis reported in Table 2 show that this increase is very significant between 3.8 and 4.2 V. The evolution of these spectra agrees with the deposition, at the very end of charging, of an important quantity of LiF, which becomes the main component of the outer part of the SEI.

P 2p spectra. The P 2p spectra of the same samples are made of two unresolved doublets ($2p_{3/2}$ and $2p_{1/2}$, with a spin-orbit splitting of about 0.8–0.9 eV). The first peak at 137.2 eV is attributed to $LiPF_6$, while the second one at 134.3 eV corresponds to the presence of phosphates due to the decomposition of $LiPF_6$. Further characterization of these phosphates is rather difficult by XPS. We can just affirm that the observed P atoms are in a four-oxygen environment, but they can be present in different forms such as PO_4^{3-} ions or $OP(OR)_3$ where *R* is an alkyl chain.[20] Upon charging, we can observe an increase of the phosphate peak intensity, which mainly occurs between 3.8 and 4.2 V. These results are in agreement with the observations of F 1s spectra. Indeed, both LiF and phosphates come from the degradation of $LiPF_6$. Therefore, the $LiPF_6$ decomposition mainly occurs between 3.8 and 4.2 V.

Li 1s spectra. The Li 1s spectra (Fig. 7) exhibit weak variations in their binding energy (between 55.7 and 56.3 eV). However, we notice a slight shift towards lower binding energies from 3.0 to 3.8 V and a shift towards higher binding energies at 4.2 V. Taking into account that the Li 1s peaks of Li_2CO_3, LiF and $LiPF_6$ are respectively located at 55.5, 56.0 and 56.9 eV, the position of the maximum depending on the composition of the Li-containing species mixture (Table 2). The progressive decrease of the binding energy up to 3.8 V is in agreement with the increase of the amount of Li_2CO_3 observed before, while the final increase in binding energy at 4.2 V is in agreement with the appearance of LiF.

Valence band spectra. To complete this analysis and to characterize more precisely the main species present in the SEI during the charge of the cell, we decided to pursue, beside the classical core peak analysis, a fine study of the valence band spectra. Recording and interpretation of these data require careful and patient experimentation but they bring out interesting information. Indeed, they scrutinize the less bound electrons of the materials (directly involved in the bonds between atoms). A detailed interpretation of an XPS valence spectrum requires the help of calculations, as it is representative of the density of states of the occupied energy levels close to the Fermi level. However, a valence spectrum can be more easily used as a fingerprint to identify a compound (or a mixture of few compounds), which constitutes a completely different approach from the core peaks analysis, and provides different information. Figure 8 displays the experimental valence spectra of samples obtained after a first charge at (a) 3.8 V and (b) 4.2 V, as well as reference spectra: (c) Li_2CO_3, (d) CH_3OCO_2Li and (e) LiF. The spectrum of Li_2CO_3 consists of a broad peak at 5–7 eV, two narrow peaks at 11 and 13 eV, and a large massif with a narrow maximum at 24–25 eV. The spectrum of CH_3OCO_2Li is very similar to that of Li_2CO_3 with a characteristic additional peak at 17.6 eV. The valence spectrum of LiF consists of a broad peak at 8–10 eV and an intense narrow peak at 29–30 eV. The spectrum of the electrode charged at 3.8 V (spectrum a)) is very close to that of Li_2CO_3. Only two differences can be noticed: (i) the peak at 29–30 eV which can be attributed to the presence of LiF, and (ii) the small peak at 17–18 eV which can be attributed to a small amount of lithium methyl carbonate CH_3OCO_2Li, as shown in a previous paper.[20] As a

result, the surface of this electrode is definitely mainly made up of Li_2CO_3 and, to a lesser extent, of LiF and CH_3OCO_2Li. These conclusions are consistent with the analysis of C 1s core peak spectra, which shows an important formation of Li_2CO_3 after charge at 3.8 V.

In the spectrum of the sample charged at 4.2 V (spectrum b), the valence shape of LiF with both main peaks at 29–30 eV and 8–10 eV can be recognized. Less clearly defined peaks can also be noticed: the massif at 22–27 eV and the small peaks at 17–18 eV, 13 eV and 5–6 eV which are consistent with the presence of CH_3OCO_2Li, or of a mixture of Li_2CO_3/CH_3OCO_2Li. As a result, the surface of this sample mainly consists of LiF and, to a lesser extent, of CH_3OCO_2Li and probably Li_2CO_3. As before, these results are in good agreement with the analysis of F 1s and C 1s core peaks spectra, and confirm a large deposit of LiF at this potential.

Note that the spectra of samples charged at 3.0 and 3.5 V are not represented in the figure, since they were more difficult to interpret, due to a more complex mixture of compounds in the passive layer.

Fifth charge

In order to study the influence of cycling on the formation of the SEI, we pursued the same study with the electrodes recovered from cells stopped during the fifth charging cycle at the same potentials.

Figure 9 shows the AFM images of electrodes stopped at (a) 3.0 V and (b) 4.2 V during the fifth charge. As shown in Fig. 9a), platelets with sharp angles can be observed again, which can be attributed to the graphite sheets, associated with amorphous-like regions assigned to the binder in the same way as at the beginning of the first charge (Fig. 6a).

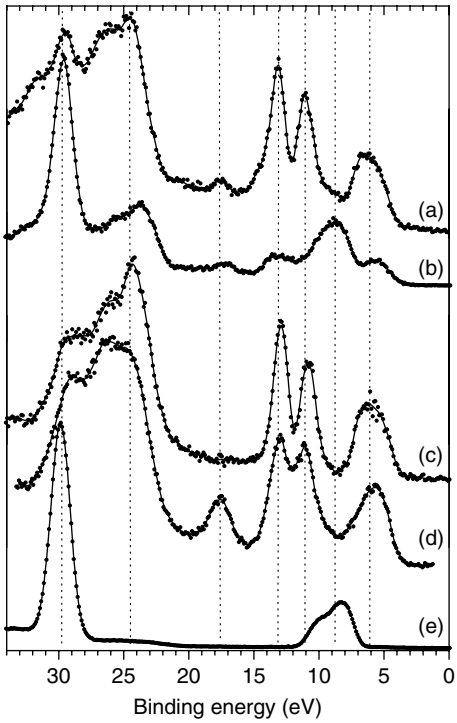

Figure 8. XPS valence spectra of the composite negative electrode stopped at: (a) 3.8 V and (b) 4.2 V, and valence spectra of reference compounds (c) Li_2CO_3 and (d) LiF.

At the end of the fifth charging (refer to Fig. 9b), the sharp angles have disappeared again, and the whole surface looks amorphous. A process of dissolution/redeposition of the surface layer is thus evidenced, at least upon the five first cycles.

The analysis of XPS core peaks spectra will allow us to get information about the nature of the species formed at the surface. Figure 10 displays the C 1s, F 1s, P 2p and Li 1s core peaks spectra of the same samples stopped at (a) 3.0 V, (b) 3.5 V, (c) 3.8 V and (d) 4.2 V during the fifth charge. This figure has to be compared to Fig. 7 corresponding to the first charge. Quantitative analysis results are reported in Table 3. Overall, the same observations can be made, except for small differences.

C 1s spectra. The C 1s spectrum of sample (a) charged at 3.0 V shows the reappearance of the graphite peak at 284.5 eV, which disappears at the end of the first charge. This confirms the AFM observations: the SEI actually partially redissolves during discharge. However, we can notice that this graphite peak is much smaller than that observed at the first charge (9% instead of 23%, Tables 2 and 3). This indicates that a very thin layer (estimated to a few nanometers) still remains at the surface of the electrode at the beginning of the 5th charge. Then, during the whole of 5th charge, we observe again a progressive decrease of this peak intensity, which reveals the progressive growth of the SEI, in good agreement with AFM observations. The thickness of the SEI seems to be greater than at the first charge, since the graphite peak totally disappears after charge at 3.8 V, while a small peak is still observed at this stage of the first charge. The species formed at this electrode–electrolyte interface are very similar to those obtained at the first charge and the same comments hold. However, we can notice that a small amount of carbonates is present at the very beginning of the charge, which suggests that carbonates do not dissolve upon discharge (Tables 2

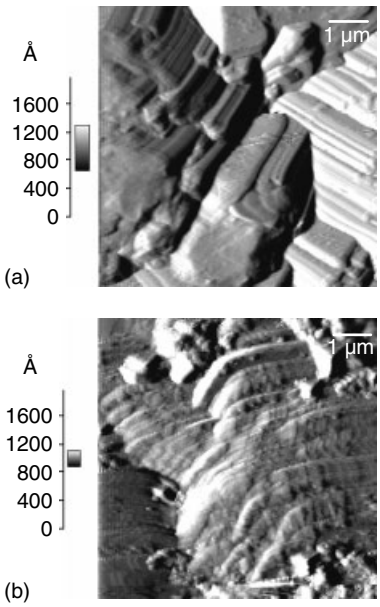

Figure 9. 10 × 10 µm^2 AFM images of the composite negative electrode stopped at (a) 3.0 V and (b) 4.2 V during the 5th charge.

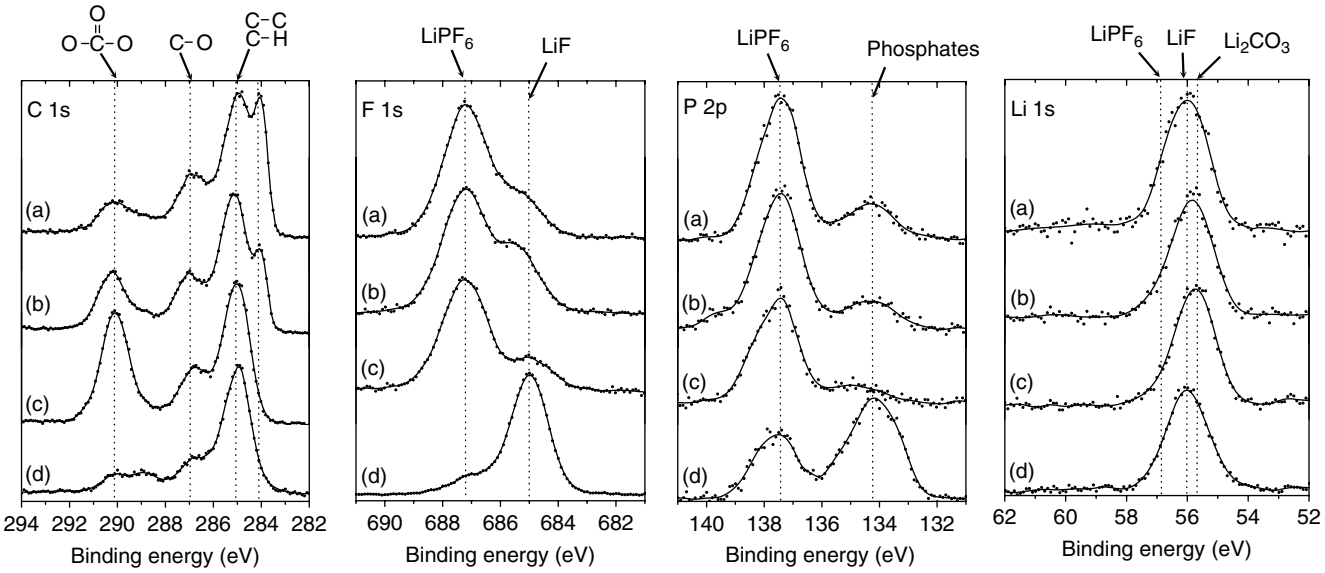

Figure 10. C 1s, F 1s, P 2p and Li 1s XPS spectra of the composite negative electrode stopped at (a) 3.0 V, (b) 3.5 V, (c) 3.8 V and (d) 4.2 V during the 5th charge.

Table 3. Binding energy (eV) and atomic percentage (%) of the elements C, O, F, P and Li from XPS spectra of the composite negative electrode as a function of the voltage of the cell during the 5th cycle (corresponding to Fig. 10)

	3.0 V		3.5 V		3.8 V		4.2 V	
Peak	BE (eV)	%	BE (eV)	%	BE (eV)	%	BE (eV)	%
C 1s	284.1	9	284.0	4	–	–	–	–
	284.9	21	285.1	19	285.0	13	285.0	16
	286.9	11	287.0	7	286.8	6	286.8	5
	288.7	2.1	288.9	1.7	288.7	1	288.9	2.4
	290.1	5.4	290.2	8	290.1	11	290.2	2
O 1s	532.0	17	532.1	23	532.3	30	532.1	17
	533.4	8	533.4	8	533.4	7	533.5	3.3
F 1s	685.2	2.2	685.3	2.4	685.1	0.8	685.0	20
	687.1	8	687.3	6	687.3	4	687.1	3.5
P 2p	134.4	0.5	134.2	0.4	134.6	0.2	134.1	1.8
	137.4	1.8	137.5	1.5	137.4	1	137.5	1
Li 1s	56.1	14	55.9	19	55.9	26	56.0	28

and 3). Furthermore, at 3.5 V, the amount of Li_2CO_3 at the fifth charge is more important than at the first charge, which is confirmed by the analysis of the valence band spectra of this sample (not shown here).

The same way as for the first cycle, we notice the presence of a small peak at 288.7–289.0 eV assignable to oxalate species (see also Table 3). This peak is easily recognizable in spectrum (d) at the end of the fifth charge.

F 1s, P 2p and Li 1s spectra. Regarding the other core peaks spectra (Fig. 10), the observations are exactly identical. We can notice the degradation of $LiPF_6$ into LiF and phosphates after charge at 4.2 V. As during the first charge at 4.2 V, the presence at this potential of a great amount of LiF at the surface, and to a lesser extent of Li_2CO_3 and CH_3OCO_2Li, is confirmed by the analysis of the valence band spectrum (not shown here).

Thus, the successive species formation that could be observed upon the first charge can be observed in the same way upon the fifth charge. This is an important result because we display a series of mechanisms that are dependent on the potential of the cell. A study limited to the beginning and the end of the charge would have only shown the formation of LiF and hidden the other processes, such as the important formation of Li_2CO_3. As a conclusion, the formation process of the SEI takes place in different successive stages as a function of the potential of the negative electrode, which is directly linked to the voltage of the full cell. At the beginning of the charge at 3.0 V, the formation of the SEI has barely started. Up to 3.8 V, the main phenomenon is the formation of Li_2CO_3 at the same time as the formation of small amounts of LiF and CH_3OCO_2Li. Finally, at the end of the charge (4.2 V) the main phenomenon is the decomposition of the salt, so that the main compound of the outer part of the SEI is LiF,

associated with a small amount of CH_3OCO_2Li and probably Li_2CO_3. Then, the SEI partially redissolves during discharge.

Several mechanisms have been previously reported that can explain the formation of Li_2CO_3 and CH_3OCO_2Li by electrochemically driven reduction the solvents:[9,21]

$$\text{EC} \quad (CH_2O)_2CO + 2\,e^- + 2\,Li^+ \longrightarrow Li_2CO_3 + C_2H_{4(g)} \tag{1}$$

$$\text{DMC } CH_3OCO_2CH_3 + 2\,e^- + 2\,Li^+ \longrightarrow Li_2CO_3 + C_2H_{6(g)} \tag{2}$$

$$\text{DMC } 2CH_3OCO_2CH_3 + 2\,e^- + 2\,Li^+ \longrightarrow 2\,CH_3OCO_2Li + C_2H_{6(g)} \tag{3}$$

$$\text{DEC } C_2H_5OCO_2C_2H_5 + 2\,e^- + 2\,Li^+ \longrightarrow Li_2CO_3 + C_4H_{10(g)} \tag{4}$$

The formation of LiF can be explained by several mechanisms reported in the literature, including reactions of the salt with trace water or with byproducts such as Li_2CO_3:[22]

$$LiPF_6 \longrightarrow LiF + PF_5 \tag{5}$$

$$PF_5 + Li_2CO_3 \longrightarrow 2\,LiF + POF_3 + CO_2 \tag{6}$$

$$LiPF_6 + H_2O \longrightarrow LiF + POF_3 + 2HF \tag{7}$$

$$LiPF_6 + Li_2CO_3 \longrightarrow 3\,LiF + POF_3 + CO_2 \tag{8}$$

$$Li_2CO_3 + 2\,HF \longrightarrow 2\,LiF + CO_2 + H_2O \tag{9}$$

However, none of reactions (5–9) is directly driven by the electrochemical lithium insertion. The formation of LiF, so important during charge between 3.8 and 4.2 V, is probably linked to the increase in acidity of the solution at the end of the charge (mainly HF or HF_2^-). Depending on the potential and the temperature, the solvent is slightly oxidized and protons are liberated at the positive electrode.[23] By migration (HF_2^-) or diffusion, these acidic species may reach the negative electrode where reaction (9) may occur. During the discharge stage, the proton generation stops and the acidity level decreases.

CONCLUSION

In this work, we could show the potential-dependent character of the formation of the species making up the SEI film at the surface of the graphite negative electrode. The formation process of the SEI takes place in different successive stages as a function of the negative electrode potential, which is directly linked to the voltage of the full cell. At the beginning of the charge at 3.0 V, the formation of the SEI has barely started. Up to 3.8 V, the main phenomenon is the formation of Li_2CO_3 at the same time as the formation of small amounts of LiF and CH_3OCO_2Li. Finally, at the end of the charge (4.2 V), the main phenomenon is the decomposition of the salt, so that the main compound of the outer part of the SEI is LiF, associated with a small amount of CH_3OCO_2Li and probably Li_2CO_3. Then, the SEI partially redissolves during discharge and the same successive species formation can be observed during the following charges. These results show that although the SEI formation is overall irreversible, a process of dissolution/redeposition of the surface layer can be evidenced, at least upon the five first cycles.

Acknowledgements

All the authors wish to thank SAFT Company for electrode manufacture and financial support. F. Blanchard would like to thank the French Regional Center for financial support.

REFERENCES

1. Winter M, Besenhard JO. In *Handbook of Battery Materials*, Besenhard JO (ed.) Wiley/VCH: Weinheim, 1999; 383.
2. Peled E. *J. Electrochem. Soc.* 1979; **126**: 2047.
3. Peled E, Golodnitsky D, Ardel G. *J. Electrochem. Soc.* 1997; **144**: L 208.
4. Zheng T, Gozdz AS, Amatucci GG. *J. Electrochem. Soc.* 1999; **146**: 4014.
5. Nazri G, Muller RH. *J. Electrochem. Soc.* 1985; **132**: 2050.
6. Aurbach D, Daroux ML, Faguy PW, Yeager E. *J. Electrochem. Soc.* 1987; **134**: 1611.
7. Aurbach D, Ein-Eli Y, Markovsky B, Zaban A, Luski S, Carmeli Y, Yamin H. *J. Electrochem. Soc.* 1995; **142**: 2882.
8. Aurbach D, Levi MD, Levi E, Schechter A. *J. Phys. Chem. B* 1997; **101**: 2195.
9. Aurbach D, Markovsky B, Weissman I, Levi E, Ein-Eli Y. *Electrochim. Acta* 1999; **45**: 67.
10. Geniès S, Yazami R, Garden J, Frison JC. *Synth. Met.* 1998; **93**: 77.
11. Andersson AM, Henningson A, Siegbahn H, Jansson U, Edström K. *J. Power Sources* 2003; **119–121**: 522.
12. Andersson AM, Herstedt M, Bishop AG, Edström K. *Electrochim. Acta* 2002; **47**: 1885.
13. Shirley DA. *Phys. Rev. B* 1972; **5**: 4709.
14. Scofield JH. *J. Electron Spectrosc. Relat. Phenom.* 1976; **8**: 129.
15. Peled E, Bar Tow D, Gladkich A, Barstein L, Golodnitsky D. *J. Power Sources* 2001; **97–98**: 52.
16. McCreery RL. Electrochemical properties of carbon surfaces. In *Interfacial Electrochemistry*, Wieckowski A (ed). Dekker: New York, 1999; 631.
17. Chagnes A, Carré B, Willmann P, Dedryvère R, Gonbeau D, Lemordant D. *J. Electrochem. Soc.* 2003; **150**: A1255.
18. Ogumi Z, Sano A, Inaba M, Abe T. *J. Power Sources* 2001; **97–98**: 156.
19. Laruelle S, Pilard S, Guenot P, Grugeon S, Tarascon J-M. *J. Electrochem. Soc.* 2004; **151**: 1202.
20. Dedryvère R, Laruelle S, Grugeon S, Gireaud L, Tarascon J-M, Gonbeau D. *J. Electrochem. Soc.* 2005; **152**: A689.
21. Fong R, Von Sacken U, Dahn JR. *J. Electrochem. Soc.* 1990; **137**: 2009.
22. Naejus R, Lemordant D, Coudert R, Willmann P. *J. Fluorine Chem.* 1998; **90**: 81.
23. Blanchard F. *Study of gas generation in lithium-ion batteries during charge or floating conditions*, PhD Dissertation, University of Tours, France, 2004.